www.czasopisma.pan.pl PAN POLSKA AKADEMIA NAUK www.journals.pan.pl

PAN ARCHIVES OF ACOUSTICS
Vol. **44**, No. 2, pp. 375–383 (2019)
DOI: 10.24425/aoa.2019.128501

Methods to Estimate the Channel Delay Profile and Doppler Spectrum of Shallow Underwater Acoustic Channels

Van Duc NGUYEN*, Tien Hoa NGUYEN, Hoa Xuan Thi HO

School of Electronics and Telecommunications
Hanoi University of Science and Technology
No 1, Dai Co Viet, Hai Ba Trung, Hanoi, Vietnam
*Corresponding Author e-mail: duc.nguyenvan1@hust.edu.vn

(*received September 30, 2016; accepted November 27, 2018*)

In this paper, we present the methods to detect the channel delay profile and the Doppler spectrum of shallow underwater acoustic channels (SUAC). In our channel sounding methods, a short impulse in form of a sinusoid function is successively sent out from the transmitter to estimated the channel impulse response (CIR). A bandpass filter is applied to eliminate the interference from out-of-band (OOB). A threshould is utilized to obtain the maximum time delay of the CIR. Multipath components of the SUAC are specified by correlating the received signals with the transmitted sounding pulse with its shifted phases from 0 to 2π. We show the measured channel parameters, which have been carried out in some lakes in Hanoi. The measured results illustrate that the channel is frequency selective for a narrow band transmission. The Doppler spectrum can be obtained by taking the Fourier transform of the time correlation of the measured channel transfer function. We have shown that, the theoretical maximum Doppler frequency fits well to that one obtained from measurement results.

Keywords: shallow underwater acoustic; channel parameters detection; channel delay profile; Doppler spectrum.

1. Introduction

In last decade years, digital underwater communication has been focalized on the design of reliable under water acoustic communication systems. It is found a wide range of applications, such as data acquisition, remote controls, submarine communication, sensor networks (Preisig, 2007; Rossi *et al.*, 2015; Song *et al.*, 2012; Stojanovic, Preisig, 2009). The underwater channel is different from the common wireless channels, when the electromagnetic waves are very strong absorbed in the highly conductive medium as water (Akada *et al.*, 2015; Babar *et al.*, 2016; Bahrami *et al.*, 2016; Binnerts *et al.*, 2017). The acoustic signals are affected in shallow-water channel by time-varying multipath channel that causes the inter-symbol interference (ISI) and Doppler shift and spread (Akada *et al.*, 2015; Qarabaqi, Stojanovic, 2013). The multipath and Doppler effects lead to the degradation of performance of underwater acoustic communication systems (Aliesawi *et al.*, 2010; Byun *et al.*, 2013; Eggen *et al.*, 2001; Kochanska, Schmidt, 2017). The different Doppler shifts are associated with scatter paths arriving at the receiver from different angles (Adzhani *et al.*, 2016; Chen *et al.*, 2016; Das, Pallayil, 2016).

The common type of the reference sounding signal today is the pseudo random sequence (PSR) or chirp signal (Cheng *et al.*, 2015; Wu *et al.*, 2012). The correlation method is applied to detect the sounding signal at the receiver. There are also a number of studies that use Delta impulse (Borowski, 2009). The use of PSR to measure underwater channel is considered to be the most accurate, however, this method requires the largest investment in hardware. Because the chirp sequence must be long enough to measure the transmission channel, leading to large overlap problems at the receiver side. Moreover, the chirp sequence must be modulated by using a suitable modulation scheme and on a carrier frequency in order to transmit a long distance in SUAC. Consequently, the demodulation problem is complex as well as the ISI is large. The very narrow Dirac pulse is hard to realize. Furthermore, the transmission the Delta impulse is only

suitable for a short communication distance. Using the Delta impulse for sounding the SUAC does not provide the good channel measurement performance, because this form of signal is strongly distorted and quickly attenuated in SUAC. Different from other studies as in (Kulhandjian, Melodia, 2014; Tomasi *et al.*, 2010; Van Walree, 2013), we use a rectangular windowed sine pulse in combination with the correlation method to detect the CIR at the receiver. Our goal consists of the following purposes: The first one is to measure the channel at a large transmission distance. In that case, the sine wave is well adopted with this requirement. Moreover, for the second purpose, the sinus signal is a form of carrier frequency, which does not require to modulate before transmission over the SUAC. Therefore, a demodulation is not necessary as if we would use the PSR method. Correlation of the received sounding signal with the transmitted rectangular windowed sinus signal will reveals the information of the CIR.

Our work will solve these aforesaid lacks by empirical measurements and analytical investigations. We consider the movement of the underwater device (UD) results in path gains, Doppler frequencies, and phase shifts which are deterministic processes instead of stochastic ones or random variables. We propose a best-fit time window based snapshot method for evaluating the CIR. This window reduces the additive noise in the time domain as well as the processing time for the channel detection. The window of the relevant measured data is calculated by comparing the received signal with the average noise threshould.

Measured environments are lakes in Hanoi, which have characteristics of shallow water. Our idea is to calculate the PDP based on determining the arrival phases of the acoustic signals as well as the multipath components of the CIR. The arrival phases of the sounding signals can be detected by correlating the transmitted signal with its linearly shifted phase from 0 to 2π, with the received signals. Although, the arrival phases of the received signal are unknown. However, the maximum correlation could show the coincidence of the shifted phase with the arrival phase of the received signal. Therefore, the arrival phases and the time delay of the multipath components of the CIR can be detected. The Doppler spectrum is obtained by taking the Fourier transform of the time correlation function of the measured channel transfer function (CTF).

The rest of this paper is organized as follows. Section 2 proposes a method to calculate the PDP of acoustic underwater channel. Section 3 describes a protocol for measuring the Doppler spectrum of received signal over shallow underwater acoustic time-varying channels. The measuremental setup is presented in Sec. 4. Section 5 presents the measurement results and discussion. We conclude the paper in Sec. 6.

2. Proposed method for determining PDPs of SUACs

The phenomena of diffraction, refraction and reflection of SUAC makes the acoustic transmission difficult (De Rango *et al.*, 2012). The properties of diffraction, reflection and refraction will affect to the number paths, path's strength and propagation delays (Stojanovic, Preisig, 2009). In this study, measurements were repeated to ensure the accuracy of the estimated channel parameters. This section describes a method to sound the power delay profiles (PDP) and the channels impulse response (CIR) $h(\tau)$ of the SUACs. The CIR can be mathematically described as (Li *et al.*, 2008; Sozer *et al.*, 2000)

$$h(\tau) = \sum_{l=1}^{L} a_l \delta(\tau - \tau_l), \tag{1}$$

where a_l and $\delta(t)$ denote the multipath amplitude and time-varying path delay for the path l-th, $l \in [1, ..., L]$, respectively. L is the total number of multipath. In order to measure the CIR $h(\tau)$, a narrow probe pulse $x(t)$, also called sounding signal, is used. The period of sending the sounding signal is T_m. The narrow probe pulse is expressed as

$$x(t) = \begin{cases} \sin(2\pi f_c t) & 0 \le t \le T_w \\ 0 & \text{otherwise,} \end{cases} \tag{2}$$

where T_w and f_c are the width and the carrier frequency of the sounding pulse, respectively. The PDP of the channel is calculated by taking the square amplitude of the CIR $|h(\tau)^2|$. The sounding signal used in the experiments is insulated in the Fig. 1. The sounding signal is repeatedly transmitted in a predetermined period T_m. Meanwhile, the CIR will be measured during these transmission periods.

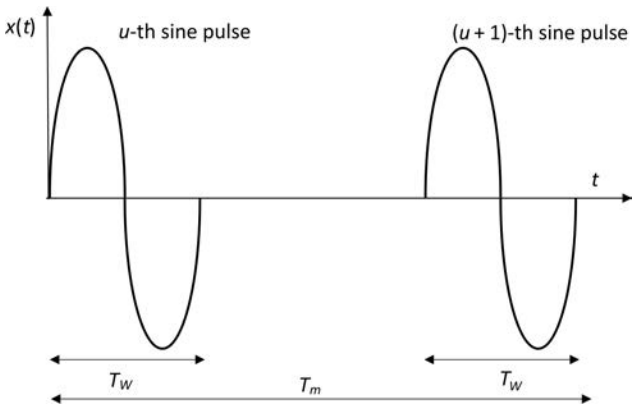

Fig. 1. A very short impulse (sounding signal) is transmitted periodically for measuring PDP of the shallow water channel.

The proposed process for determining the PDP of shallow underwater channel involves three steps. The

flowchart of this process is illustrated in the Fig. 2. These three steps of this process are described as follows:

Step 1: Noise elimination by using band-pass filter

The out-of-band noises introduced in the received signals are eliminated by using a band-pass filter. The bandwidth of the filter is designed to cover the data rate of the sounding signal.

Step 2: A proposed best-fit time window for PDP calculating

The purpose to determine the relevant window (RWin) of the received signal in the time domain is to eliminate the noise in the time domain, as well as to reduce the processing time and to get more precise information in terms of the channel parameters. This window is defined by a starting time t_u^{b} and an ending time t_u^{e}, where the index u denotes the u-th period of measurement. This period corresponds to the sine sounding period as depicted in Fig. 1. The staring time t_u^{b} is the first instant time, when the received signal power is larger than a given threshould P_{thr}, which is in practice determined on the basic of the measured additive noise power. The ending time t_u^{e} is the last time instant, that the received signal power is larger than the threshould power P_{thr}. The P_{thr} depends on the noise level of the measuring that based on the level of noise in the environment, which can be obtained by listening in the absence of signals. In other words, the RWin specifies a window that the received signal power is equal or larger than the measured additive noise power.

Figure 1 illustrates the transmitted sounding signal $x(t)$ in several period of measurements. At the receiver, the received sounding signal is expressed as follow:

$$y(t) = x(t) * h(\tau) + n(t), \tag{3}$$

where $y(t)$, $n(t)$ are the received sounding signal, the additive coloured noise, respectively. To describe the mathematical description of our method to determine the RWin for each measurement period, let $y_u(t)$ denote the received sounding signal observed within the time window $uT_m \le t \le (u+1)T_m$. Firstly, we calculate the power $P_u(t)$ of the digital signal at the receiver side as follows

$$P_u(t) = |y(t)|^2 \quad \text{for} \quad uT_m \le t \le (u+1)T_m. \tag{4}$$

Secondly, the signal power $P_u(t)$ will be compared to the average noise level P_{thr} within the width of window RWin. This process is mathematically presented as follows

$$\begin{aligned} &\text{Seeking} \quad t_n = \{P_u(t) > P_{\mathrm{thr}}\} \\ &\text{subject to:} \quad uT_m \le t_n \le (u+1)\,T_m. \end{aligned} \tag{5}$$

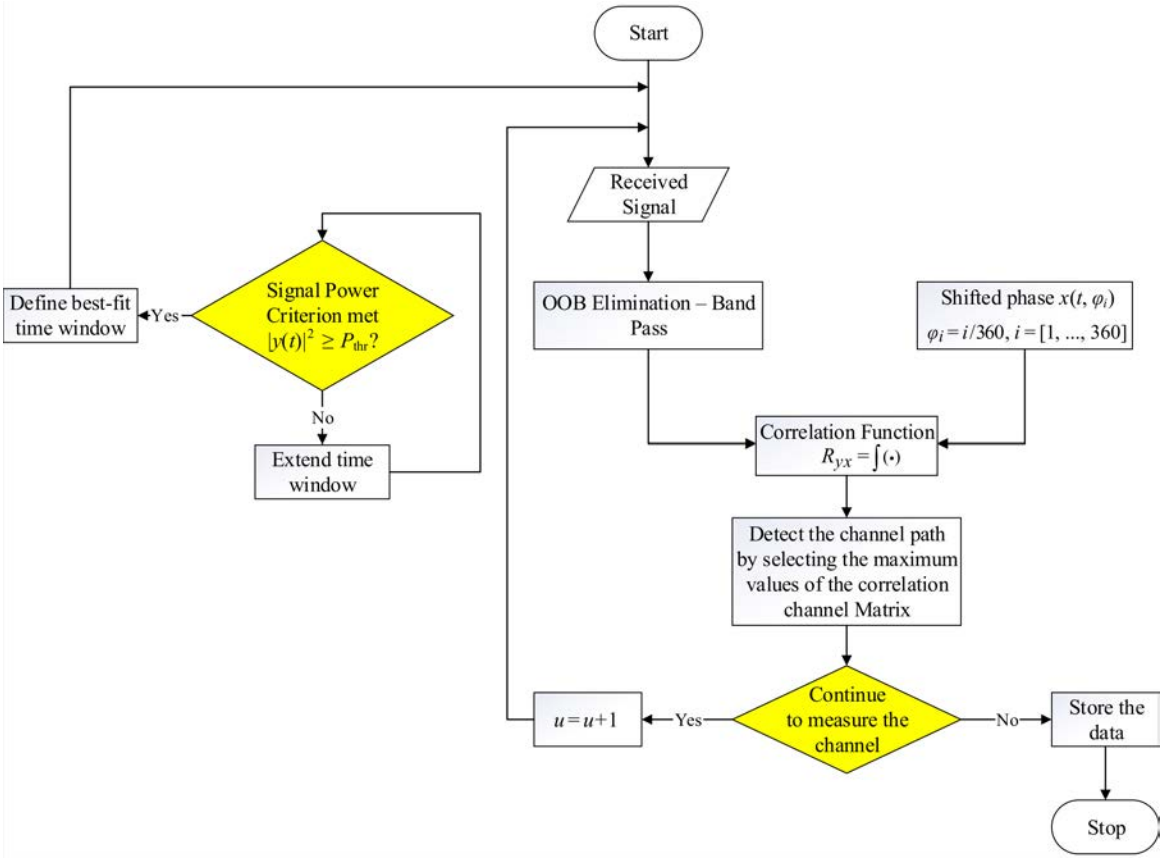

Fig. 2. Best-fit time windowing method combined with correlation for maximum PDP and Doppler detection.

In the corresponding time of window RWin, the starting time is determined by seeking the minimum value of t_n

$$t_u^{\mathrm{b}} = \min\{t_n\}, \tag{6}$$

and the ending time of the RWin t_u^{e} is defined by the maximum value of t_n

$$t_u^{\mathrm{e}} = \max\{t_n\}. \tag{7}$$

Based on t_u^{e}, we can calculate the maximum time delay of the CIR of the u-th measurement, $\tau_{\max,u}$ as

$$\tau_{u,\max} = t_u^{\mathrm{e}} - uT_m. \tag{8}$$

According to the obtained RWin, we capture the relevant received signal $y_{r,u}(t)$ to determine the multipath components of the CIR as following

$$y_u(t) = \begin{cases} y(t) & t_u^{\mathrm{b}} \le t \le t_u^{\mathrm{e}}, \\ 0 & \text{otherwise.} \end{cases} \tag{9}$$

After removing the presence of out-band noise in frequency domain as introduced in the step 1, as well as the additive noise out of the RWin in the time domain as proposed in the step 2, we estimate the multipath components of the channel by using the correlation technique as described in the following step.

Step 3: Determine the Multipath Components of the SUAC

In this step, we proposed a method to estimate the multipath components of the SUAC by correlating the received sounding signal with the transmitted sounding signal. The idea of the method is based on the correlation of the received signal with the transmitted sinusoid sounding signal. However, the phase this sounding signal is linearly shifted as given in the mathematical form below (Dunn, 2005):

$$R_{yx}^{(u)}(t', \varphi_j) = \int_{-\infty}^{\infty} y_u(t+t') \cdot x(t, \varphi_j) \quad \text{for} \quad 0 \le t' \le T_w + \tau_{\mathrm{u,max}}, \tag{10}$$

where $T_w = W \cdot t_a$, and $\tau_{u,\max} = L_{u,\mathrm{e}} \cdot t_a$. The symbols $t_a = 1/f_s$, W, and $L_{u,\mathrm{e}}$ denotes the sampling interval, the number of sampling intervals within the duration of the sinusoid sounding pulse, and within the $\tau_{u,\max}$, respectively. The transmitted sounding signal $x(t)$, with phase shifted by φ_j, can be expressed as

$$x(t, \varphi_j) = \begin{cases} \sin(2\pi f_c t + \varphi_j) & 0 \le t \le T_w, \\ 0 & \text{otherwise,} \end{cases} \tag{11}$$

where the shifted phase

$$\varphi_j = j2\pi/M \qquad \text{with} \qquad j \in [0, 1, ..., M-1].$$

M is the number of shifted phases, which can be chosen for the desired accuracy level. In this work, we set $M = 360$, corresponding to each phase shift step is 1°. The received sounding signal $y_u(t)$ consists of the signals from L different channel paths. Each path has different arrival phase, which depends on the transmission environment. If the shifted phase coincides with the arrival phase of a channel path, the cross-correlation function in Eq. (10) shows its local maximum at $t' = 0$. By searching this local maximum, we can detect the channel path information, which includes the propagation delay, attenuation factor, and the corresponding phase delay of the detected channel path. In addition, the authors in (Vriens, Janssen, 1991) have proved, that the channel attenuation factor of the channel path is proportional to the maximal value of the cross-correlation function $R_{yx}^{(u)}(t', \varphi_j)$.

In the following, we describe how to extract the channel information from the cross-correlation function given in Eq. (10). For simplicity, but without loss of generality, we neglect the measurement index u for our further presentation. The received signal in fact is digitalized by the ADC before it can be processed at the receiver. Thus, we replace the continuous time variable by the discrete time, i.e. $t = t_k$ with $t_k = k \cdot t_a$, where k denotes the sampling index. The cross-correlation function must be also presented in the discrete form. For a given shifted phase φ_j, we can rewrite the cross-correlation function of the received signal given in Eq. (10) in discrete form as follow

$$R_{yx}[k, \varphi_j] := R_{yx}[t'_k, \varphi_j]. \tag{12}$$

For $0 \le k \le W + L_{\mathrm{e}} - 1$, we obtain the following correlation vector

$$\mathbf{R}_{yx}(\varphi_j) = [R_{yx}(0, \varphi_j), ..., R_{yx}(k, \varphi_j), ..., R_{yx}(N-1, \varphi_j)]_{1\times N}, \tag{13}$$

where $N = W + L_{\mathrm{e}}$ is the length of the correlation vector. For all $\varphi_j \in [0, \ldots, (M-1) \cdot 2\pi/M]$, the cross-correlation matrix can be formed by

$$\mathbf{R}_{yx} = \begin{bmatrix} \mathbf{R}_{yx}(\varphi_0) \\ \mathbf{R}_{yx}(\varphi_1) \\ \cdots \\ \mathbf{R}_{yx}(\varphi_{M-1}) \end{bmatrix}_{M\times N}. \tag{14}$$

Observing the l-th column of the matrix $\mathbf{R}_{yx}$, we can find a row, whereby its value is maximum

$$R_{yx}(l, \varphi_m) = \max\left(\begin{bmatrix} R_{yx}(l, \varphi_0) \\ R_{yx}(l, \varphi_1) \\ \cdots \\ R_{yx}(l, \varphi_{M-1}) \end{bmatrix}_{M\times 1} \right). \tag{15}$$

This row is indexed by m. The corresponding shifted phase is φ_m. Based on the characteristic of the cross-

correlation function, the shifted phase φ_m must be coincided with the arrival phase corresponding to the time index l. In other words, the arrival phase of the l-th path has been detected, and is denoted by $\widehat{\varphi}_l := \varphi_m$. $R_{yx}(l;\varphi_m)$ reveals the information of the propagation delay, which relates to the shifted phase. By searching for all maximum values of all rows of the matrix $\mathbf{R}_{yx}$, we obtain the following vector

$$\mathbf{r}_{yx} = [R_{yx}(0,\widehat{\varphi}_0),...,R_{yx}(k,\widehat{\varphi}_k),..., R_{yx}(N-1,\widehat{\varphi}_{N-1})]_{1\times N}. \quad (16)$$

Based on the vector $\mathbf{r}_{yx}$, the discrete CIR of one period of measurement is detected. The sounding signal $x(t)$ has a width of T_m seconds, which corresponds to W sampling intervals. Using the sounding impulse with its width of T_m, we are able to detect the channel taps with their resolution larger than T_m. In other words, the gaps between two channel taps should be larger than T_m. Otherwise, the received sounding signals will be overlapped to each other due to the multipath propagation. Thus, we split the vector $\mathbf{r}_{yx}$ into number of consecutive groups, whereas each group consist W elements. The maximum value of each group corresponds to the channel coefficient and the time delay of the main channel path located in this group.

3. A protocol to detect the Doppler spectrum based on the measured CIR

The time correlation function (TCF) of the channel $\Psi_{HH}(\Delta t)$ can be expressed as (Proakis, 2007)

$$\Psi_{HH}(\Delta t) = E[H^*(f_c,t), H(f_c,t+\Delta t)], \quad (17)$$

where the channel transfer function $H(f,t)$ is the Fourier transform of the channel impulse response $h(\tau,t)$. Because time-varying channels are considered in this section, the observed time (or absolute time) t is included in the presentation of the channel transfer function (CTF). The Doppler power spectrum is the Fourier transform of the time correlation function (TCF) of the CTF, which is given as follows (Proakis, 2007)

$$\Phi_{yy}(f) = \int \Psi_{HH}(\Delta t) e^{(-j2\pi f \Delta t)}\, \mathrm{d}(\Delta t). \quad (18)$$

To estimate the Doppler spectrum of the SUACs from the measured CIR, we need firstly obtain the CTFs $H(f,t)$. Afterwards, the TCF in Eq. (17) is computed. Finally, the Doppler spectrum of the SUACs is calculated by using the relation given in Eq. (18).

4. Experimental setup

4.1. Hardware implementation

In this work, we used a self-designed circuit to generate pulses of 173 and 200 kHz as in Fig. 3a generating the sounding pulses. The pulses are modulated from the circuit will be fed to the amplifier and resonant circuit in Fig. 3b successively. The modulated sounding signal has been shown in Fig. 3c. Then, we use the BII-7562 transducer to transmit the output signals in Fig. 3d. The resonant voltage with the transducer is 200 V and the input power is nearly 600 W. It is important to have the input power of 600 W for long range transmission.

The sounding signal is received by using another transducer, which works well at the frequency 173 and 200 kHz, see Fig. 3e. The received signal is consecutively amplified, filtered by a band-pass filter, and passed to an envelope extractor as in Fig. 3f–h.

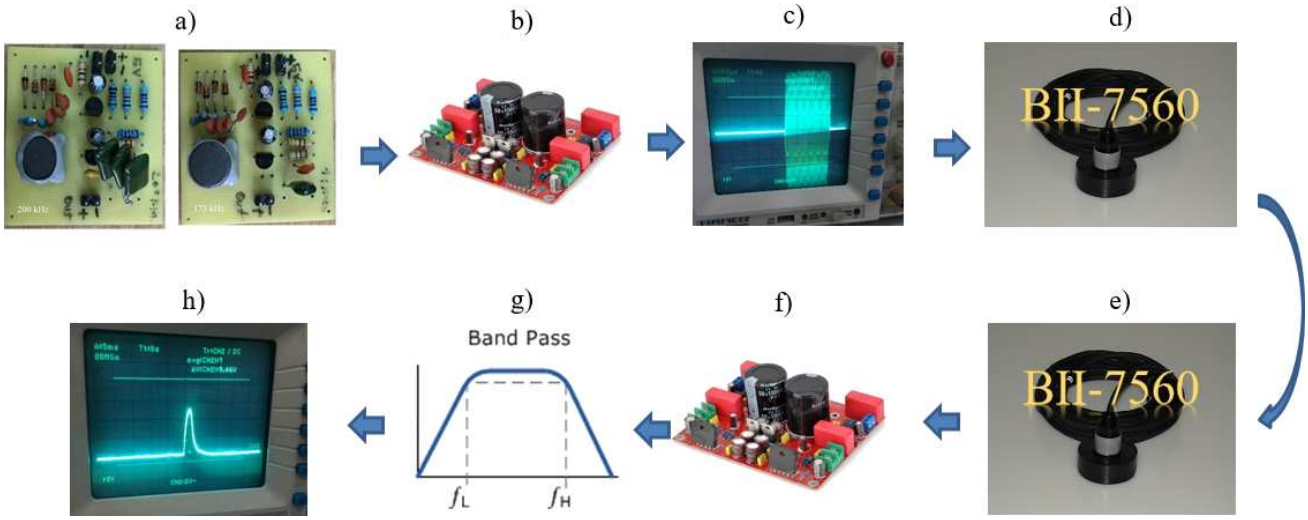

Fig. 3. Model of shallow underwater channel measurement conducted in Hanoi lakes.

4.2. Experimental setup for measuring the Doppler characteristics

The experiments were conducted in the Thongnhat lake in Hanoi to measure the impulse response of the shallow underwater acoustic channel. The Thongnhat lake has slightly flat bottom and a depth of up to 3 m. Transducer and Hydrophone are set up securely at depth 0.5 m. To measure the PDP of static channels, the transmitter and the receiver are kept to be almost static. The experimental system is captured in Fig. 4.

Fig. 4. A picture of the Thongnhat lake, where experiments have been carried out.

The experimental setup for the receiver is depicted in Fig. 4, setup for the transmitter is also similar to the receiver deployment.

The detail parameters for the experiment setup are shown in Table 1, where the transducer and the hydrophone are sank in the water with the depth of 0.5 m below the water surface. The sounding signal for channel measurement is a very short sinus impulse depicted in Fig. 1, with its width of $T_w = 1/14$ ms, and is sent out with a period of $T_m = 0.5$ s.

Table 1. Parameters of experimental system.

Parameters	Value
Depth of T_x and R_x	0.5 m
Carrier frequency (f_c)	14 kHz
Pulse width of the sounding signal (T_w)	1/14 ms
Period of sending the sounding signal (T_m)	0.5 s
Sampling frequency (f_s)	192 kHz
Distance from T_x to R_x (d)	150 m
Bandwidth of the measured channel B	7 kHz
Sampling interval ($t_a = 1/f_s$)	5.2 µs

The experimental setup for measuring the Doppler characteristics of the received signal for the case that there is a relative movement between the transmitter and the receiver, is similar to that for measuring the characteristics of static channels. However, the difference is that the receiver moves around the transmitter. The relative movement speed between the transmitter and the receiver is about 15 km/h. The receiver deployment for the Doppler characteristics measurement is shown in Fig. 4.

5. Measurement results and discussion

5.1. The obtained CIR by using proposed method for a static channel

After noise filtering and taking only values falling in the relevant window, the received sounding signal is plotted in Fig. 5. Applying the correlation of the received signal with the transmitted signal as introduced in Sec. 2, we obtain the CIRs $h(\tau, t)$ as plotted in Fig. 6.

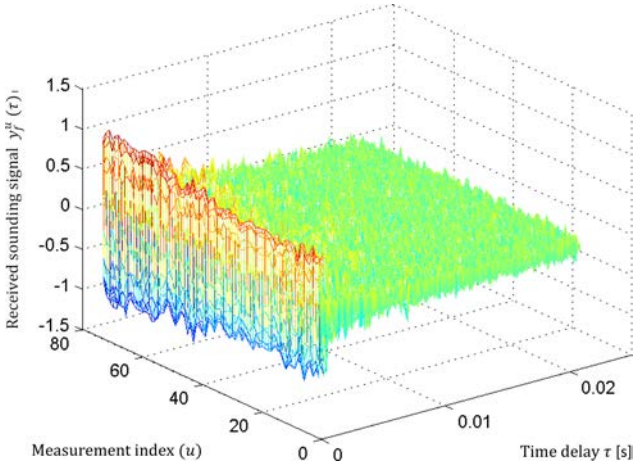

Fig. 5. The received sounding signal over a static underwater channel measured in Thongnhat lake.

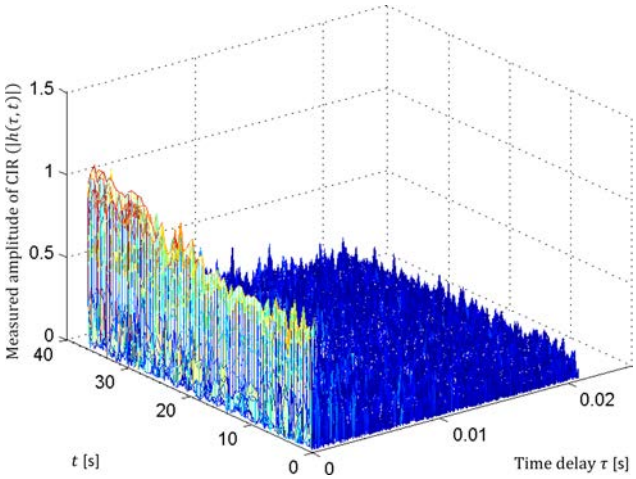

Fig. 6. The amplitude of the CIR measured in Thongnhat lake in a condition of quasi-static environment.

The CTF $H(f,t)$ is the Fourier transform of the CIR $h(\tau,t)$, and is displayed in Fig. 7. Finally, the channel delay profile of the channel is the mean of the amplitude square of the CIR, as depicted in Fig. 8. We can observe that the maximum time delay of the channel is 5–6 ms compared to the first arrival path. Please be aware that we have neglected the group delay, and therefore set the propagation time delay of the first arrival path to be zero.

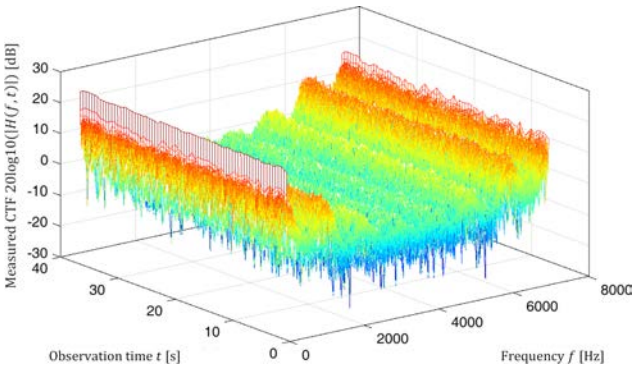

Fig. 7. The CTF of a static channel measured in Thongnhat lake.

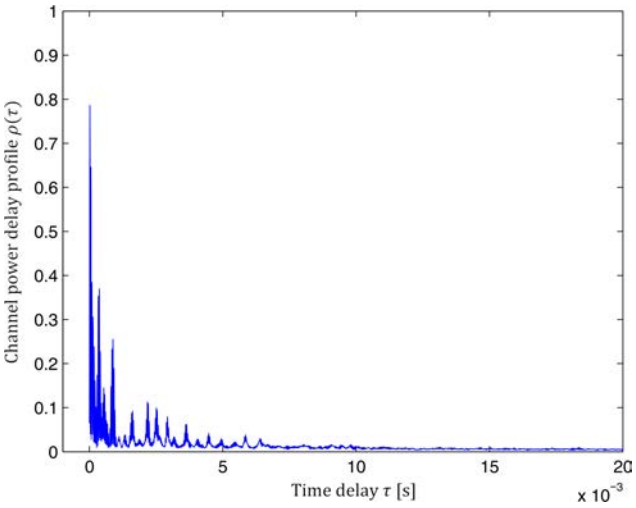

Fig. 8. The PDF of the SAUC measured in Thongnhat lake in Hanoi.

5.2. Estimated Doppler spectrum using the proposed protocol for a fast time-varying channel

To measure the Doppler spectrum, we use the same sounding signal as given in Fig. 1 to estimate the CIR. A period of the received signal before noise filtering is plotted in Fig. 9. It is to recognize that the received signal is included with noises and multipath components. We deploy the band pass filter to eliminate the OOB noise, where the results are illustrated in Fig. 10.

Similar to the static channel measurement, we use the channel sounding method described in Sec. 2 to obtain the CTF. The time correlation function of the

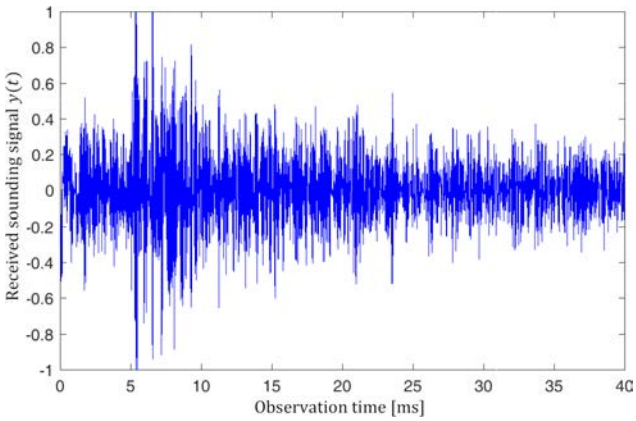

Fig. 9. A sequence of received pulses if the narrow signal pulse is transmitted with a period of transmitting of 40 ms.

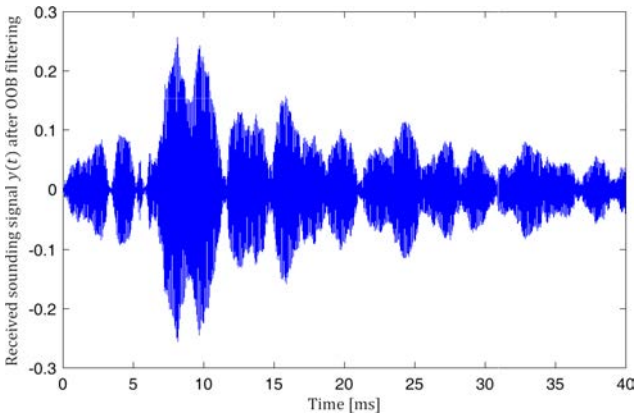

Fig. 10. Received signal sample after filtering.

channel can be obtained by applying the Eq. (17), whereby the CTF of $H(f_o,t)$ is the CTF at an observed frequency. f_o could be any frequency falling in areas of the channel bandwidth. The obtained time correlation function of the channel is plotted in Fig. 11. Finally, the Doppler spectrum of the channel is obtained by taking the Fourier transform of the TCF of the channel as given in Eq. (18). The obtained Doppler

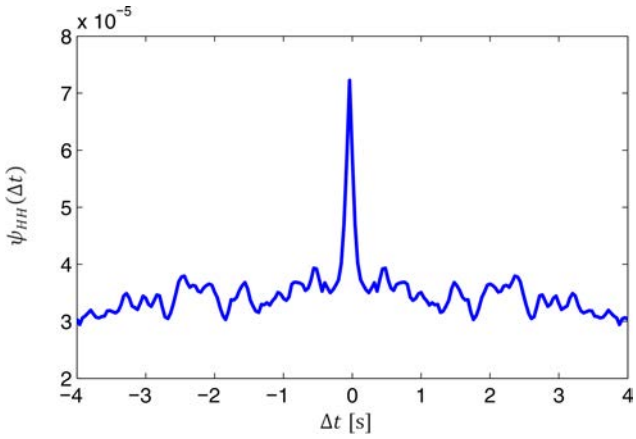

Fig. 11. Time correlation function of the measured channel.

spectrum is shown in Fig. 12. We can see that the maximum Doppler frequency is about 12.5 Hz. In the theory, the relation between the maximum Doppler frequency f_{Dmax}, the speed of acoustic sound in underwater c, and the carrier frequency f_c are given by

$$f_{\mathrm{Dmax}} = \frac{v}{c} f_c. \tag{19}$$

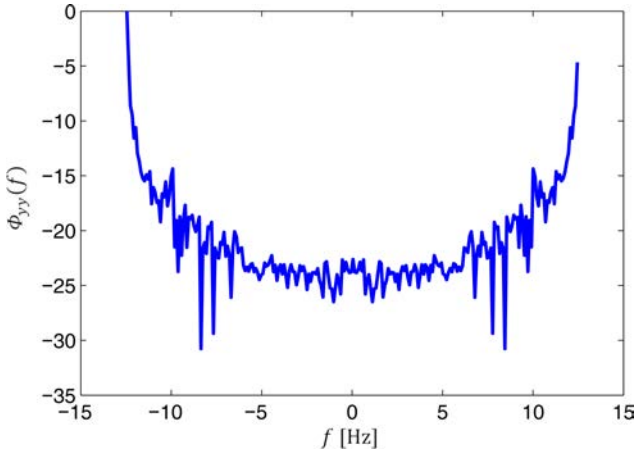

Fig. 12. The Doppler spectrum of the underwater acoustic channel.

Replacing the values of the carrier frequency given in Table 1, the speed of acoustic sound in underwater c = 1500 m/s, and the relative movement speed between the receiver and the transmitter v = 5 km/h, we obtained the maximum Doppler frequency f_{Dmax} = 12 Hz. This calculation result fit well to our measured result in terms of the maximum Doppler frequency.

6. Conclusions

In this paper, we have introduced the methods to detect the PDP and the Doppler spectrum of the SUACs. A short rectangular windowed sine signal is used as a sounding signal. This shape of sounding signal is suitable for SUAC transmission, because the frequency and amplitude are constant. In our proposed method, the CIR can be detected by correlating the received sounding signal with the transmitted ones, but its phase is linearly shifted from 0 to 2π. The maximum correlation values show us multipath components of the channel. We have applied this method to measure the underwater channel in the Thongnhat lake in Hanoi. The measurement results show that the channel is strongly affected by the additive noise. Moreover, the channel is frequency selective due to slow transmission speed of the acoustic signal in underwater, as well as the reflection and scattering effect. The Doppler spectrum can be obtained by taking the Fourier transform of the time correlation function of the CTF. The maximum Doppler frequency taken from the Doppler spectrum fit well to the theoretical results.

Acknowledgment

This material is based upon work supported by Vietnams National Foundation for Science and Technology Development (NAFOSTED) under Grant No. 102.04-2018.12.

References

1. Adzhani S.I., Mahmudah H., Santoso T.B. (2016), *Time-frequency analysis of underwater ambient noise of mangrove estuary*, [in:] International Electronics Symposium (IES), pp. 223–227.
2. Akada S., Yoshizawa S., Tanimoto H., Saito T. (2015), *Experimental evaluation of data selective rake reception for underwater acoustic communication*, [in:] 2015 International Symposium on Intelligent Signal Processing and Communication Systems (ISPACS), Nusa Dua, pp. 514–519.
3. Aliesawi S., Tsimenidis C.C., Sharif B.S., Johnston M. (2010), *Efficient channel estimation for chip multiuser detection on underwater acoustic channels*, [in:] 7th International Symposium on Communication Systems, Networks & Digital Signal Processing (CSNDSP 2010), pp. 173–177.
4. Babar Z., Sun Z., Ma L., Qiao G. (2016), *Shallow water acoustic channel modeling and OFDM simulations*, [in:] OCEANS 2016 MTS/IEEE Monterey, pp. 1–6.
5. Bahrami N., Khamis N.H.H., Baharom A.B. (2016), *Study of underwater channel estimation based on different node placement in shallow water*, IEEE Sensors Journal, **16**, 4, 1095–1102.
6. Binnerts B., Blom K., Giodini S. (2017), *Analysis of underwater acoustic propagation in a harbour environment and its effect on communication*, [in:] OCEANS 2017 – Aberdeen, pp. 1–6.
7. Borowski B. (2009), *Characterization of a very shallow water acoustic communication channel*, [in:] OCEANS 2009, Biloxi, MS, pp. 1–10.
8. Byun S.H., Seong W., Kim S.M. (2013), *Sparse underwater acoustic channel parameter estimation using a wideband receiver array*, IEEE Journal of Oceanic Engineering, **38**, 4, 718–729.
9. Chen Y., Zou L., Zhao A., Yin J. (2016), *Null subcarriers based Doppler scale estimation for multicarrier communication over underwater acoustic non-uniform Doppler shift channels*, [in:] IEEE/OES China Ocean Acoustics (COA), pp. 1–6.
10. Cheng E., Chen S., Yuan F. (2015), *Design and detection of multilinear chirp signals for underwater acoustic sensor networks*, International Journal of Distributed Sensor Networks, **2015**, Article ID 371579, doi: 10.1155/2015/371579.
11. Das A., Pallayil V. (2016), *Validation of channel model for evaluating the performance of probing signal design in shallow tropical waters*, [in:] OCEANS 2016 MTS/IEEE Monterey, pp. 1–6.

12. De Rango F., Veltri F., Fazio P. (2012), *A multipath fading channel model for underwater shallow acoustic communications*, [in:] IEEE International Conference on Communications (ICC), pp. 3811–3815.
13. Dunn P.F. (2005), *Measurement and data analysis for engineering and science*, New York: McGraw-Hill.
14. Eggen T., Preisig J., Baggeroer A. (2001), *Communication over Doppler spread channels. II. Receiver characterization and practical results*, IEEE Journal of Oceanic Engineering, **26**, 4, 612–621
15. Kochanska I., Schmidt J. (2017), *Probe signal processing for channel estimation in underwater acoustic communication system*, [in:] Signal Processing: Algorithms, Architectures, Arrangements, and Applications (SPA), Poznan, pp. 325–330.
16. Kulhandjian H., Melodia T. (2014), *modeling underwater acoustic channels in short-range shallow water environments*, [in:] Proceedings of the International Conference on Underwater Networks & Systems (WUWNET), pp. 26:1–26:5, ACM, New York, NY, USA, Article 26.
17. Li B., Zhou S., Stojanovic M., Freitag L., Willett P. (2008), *Multicarrier communication over underwater acoustic channels with nonuniform Doppler shifts*, IEEE Journal of Oceanic Engineering, **33**, 2, 198–209.
18. Preisig J. (2007), *Acoustic propagation considerations for underwater acoustic communications network development*, ACM SIGMOBILE Mobile Computing and Communications Review, **11**, 4, pp. 2–10.
19. Proakis J. (2007), *Digital communications* (5th ed.), pp. 830–898, New York: McGraw-Hill.
20. Qarabaqi P. Stojanovic M. (2013), *Statistical characterization and computationally efficient modeling of a class of underwater acoustic communication channels*, IEEE Journal of Oceanic Engineering, **38**, 4, 701–717.
21. Rossi P.S., Ciuonzo D., Ekman T., Dong H. (2015), Energy detection for MIMO decision fusion in underwater sensor networks, IEEE Sensors Journal, **15**, 3, 1630–1640.
22. Song X., Willett P., Glaz J., Zhou S. (2012), *Active detection with a barrier sensor network using a scan statistic*, IEEE Journal of Oceanic Engineering, **37**, 1, 66–74.
23. Sozer E.M., Stojanovic M., Proakis J.G. (2000), *Underwater acoustic networks*, IEEE Journal of Oceanic Engineering, **25**, 1, 72–83.
24. Stojanovic M., Preisig J. (2009), *Underwater acoustic communication channels: Propagation models and statistical characterization*, IEEE Communications Magazine, **47**, 1, 84–89.
25. Tomasi B., Zappa G., McCoy K., Casari P., Zorzi M. (2010), *Experimental study of the space-time properties of acoustic channels for underwater communications*, [in:] OCEANS 2010 IEEE – Sydney, pp. 1–9.
26. van Walree P.A. (2013), *Propagation and scattering effects in underwater acoustic communication channels*, IEEE Journal of Oceanic Engineering, **38**, 4, 614–631.
27. Vriens J., Janssen G. (1991), *Radio channel measurements using a broadband pseudo-noise signal (measurement set-up and processing of the results)*, [in:] Final Report Physics and Electronics Lab. TNO, pp. 101.
28. Wu L. *et al.* (2012), *Designing an adaptive acoustic modem for underwater sensor networks*, IEEE Embedded Systems Letters, **4**, 1, 1–4.